Material Factors

H.K.D.H. Bhadeshia, University of Cambridge

RESIDUAL STRESSES are a consequence of interactions among time, temperature, deformation, and microstructure (Fig. 1). Material or material-related characteristics that influence the development of residual stress include thermal conductivity, heat capacity, thermal expansivity, elastic modulus and Poisson's ratio, plasticity, thermodynamics and kinetics of transformations, mechanisms of transformations, and transformation plasticity.

Many general statements can be made about the role of material factors in the evolution of residual stress. Spatial variations in temperature give rise to nonuniform thermal strains, the effect of which becomes exaggerated when the material is elastically stiff and has a high yield strength. A large thermal conductivity helps reduce residual stress by reducing temperature gradients (Ref 2). The dissipation or absorption of heat depends not only on the external environment of the component but also on internally generated heat—for example, during adiabatic deformation or due to the latent heat of transformation. Similarly, the plastic strain distribution in the component depends both on the constitutive properties and on how the shape deformations due to phase transformations compensate for the development of stress.

The fundamental material properties are, of course, temperature dependent. Table 1 illustrates how several key properties might vary with temperature (Ref 3). Some of these properties, which can to some extent be estimated quantitatively, are discussed in detail in the sections that follow; others such as elastic modulus and thermal conductivity still have to be measured for individual alloys.

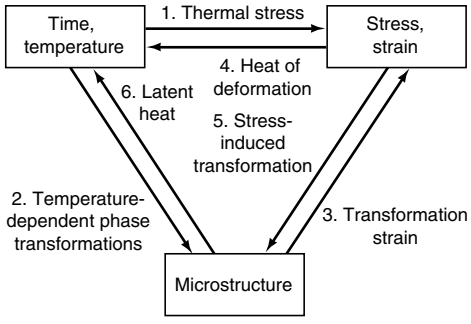

Fig. 1 The coupling of temperature, stress, and microstructure. Source: Ref 1

Heat Capacity

The dominant contribution to specific heat capacity comes from lattice vibrations (phonons), since the majority of free electrons are prevented from participation in heat absorption by the Pauli exclusion principle. However, for iron and its alloys, a further important contribution comes from magnetic changes. The net specific heat capacity can therefore be factorized into three components:

$$C_P\{T\} = C_V^L\left\{\frac{T_D}{T}\right\}C_1 + C_eT + C_P^\mu\{T\} \qquad \text{(Eq 1)}$$

where $C_V^L\{T_D/T\}$ is the Debye specific heat function and T_D is the Debye temperature. The function C_1 corrects $C_V^L\{T_D/T\}$ to a specific heat at constant pressure. C_e is the electronic specific heat coefficient, and C_P^μ is the component of the specific heat capacity due to magnetism. Figure 2 illustrates the data for ferrite and austenite in pure iron. Whereas it is well known that ferrite undergoes a paramagnetic to ferromagnetic transition on cooling below 1042.15 K, the magnetic properties of austenite are seen from Fig. 2 to be of some consequence in determining the heat capacity. There are two coexisting electron states of austenite, one of which is ferromagnetic with a Curie temperature of 1800 K and the other of which is antiferromagnetic with a Néel temperature of 55 to 80 K (Ref 4). The balance between these states changes with temperature, giving rise to corresponding changes in heat capacity.

The data in Fig. 2 are for pure iron, but there is now sufficient understanding of the components of heat capacity to enable similar estimates for iron alloys, using internationally available computer programs and thermodynamic data-

Table 1 Physical properties that affect the development of residual stress in steels

Property	Phase(a)	Temperature, °C (°F)			
		0 (32)	300 (570)	600 (1110)	800 (1470)
Elastic modulus, GPa	γ	200	175	150	124
	α + P	210	193	165	120
	α_b	210	193	165	120
	α′	200	185	168	. . .
Poisson ratio	γ	0.291	0.309	0.327	0.345
	α + P	0.280	0.296	0.310	0.325
	α_b	0.280	0.296	0.310	0.325
	α′	0.280	0.296	0.310	. . .
Thermal expansivity, K^{-1}	γ		2.1×10^{-5}		
	α + P		1.4×10^{-5}		
	α_b		1.4×10^{-5}		
	α′		1.3×10^{-5}		
Thermal conductivity, W/m · K	γ	15.0	18.0	21.7	25.1
	α + P	49.0	41.7	34.3	27.0
	αb	49.0	41.7	34.3	27.0
	α′	43.1	36.7	30.1	. . .
Specific heat capacity, 10^{-6} J/m^3 · K	γ	4.15	4.40	4.67	4.90
	α + P	3.78	4.46	5.09	5.74
	α_b	3.78	4.46	5.09	5.74
	α′	3.76	4.45	5.07	. . .
Yield strength, MPa	γ	190	110	30	20
	α + P	360	230	140	30
	α_b	440	330	140	30
	α′	1600	1480	1260	. . .

(a) α, P, α_b, and α′ represent allotriomorphic ferrite, pearlite, bainite, and martensite, respectively. Source: Ref 3

bases (Ref 6). After all, changes in fundamental thermodynamic quantities such as enthalpy and entropy are derived from heat capacity data. It is surprising that this capability has not yet been exploited in any calculation of residual stress, even though the methodology is widely available.

Expansion Coefficient and Density

Table 1 shows that the expansion coefficient of austenite is larger than that of ferrite; this might be considered surprising given the lower density of ferrite. However, the behavior is again a reflection of the two coexisting electronic states of austenite (γ_0 and γ_1), each with a thermal expansion coefficient that is identical to that of ferrite. The γ_0 component has the lower molar volume and is the antiferromagnetic form, whereas the denser γ_1 form is ferromagnetic. The relative proportion of atoms in the γ_0 and γ_1 states changes with temperature, so that the apparent expansion coefficient of austenite as a whole, as detected experimentally, is much larger than that of ferrite (Fig. 3).

The molar volumes (in cm^3/mol) of γ_0, γ_1, γ, and α over the temperature range of 300 to 1775 K are:

$$V_m^{\gamma_0} = 6.695(1 + 2.043 \times 10^{-5}T + 1.52 \times 10^{-8}T^2)$$

$$V_m^{\gamma_1} = 7.216(1 + 2.043 \times 10^{-5}T + 1.52 \times 10^{-8}T^2)$$

$$V_m^{\gamma}\{T\} = (1 - y)V_m^{\gamma_0}\{T\} + y\,V_m^{\gamma_1}\{T\}$$

$$V_m^{\alpha}\{T\} = 7.061(1 + 2.043 \times 10^{-5}T + 1.52 \times 10^{-8}T^2)$$

where y is the fraction of atoms of austenite in the γ_1 state, the details of which can be found elsewhere (Ref 4, 5).

These data are for pure iron, but thermodynamic data can be used to assess how the expansion coefficients would change with alloying, since there are quite sophisticated treatments of the effect of solute elements on the magnetic and other components of the free energies of iron. Note that the "two electronic states" picture of austenite is a simplification of the real scenario, but first-principles calculations (Ref 7), which deal with higher levels of complexity, are not yet applicable to practical alloys.

Plastic Deformation

The familiar mechanisms of plastic deformation are slip, mechanical twinning, and creep. Phase transformations also cause permanent deformation (Ref 8–11). In steels, austenite can decompose into a large variety of microstructures that are distinguished by the atomic mechanism of transformation (Fig. 4). In a displacive transformation, the change in crystal structure is achieved by a deformation of the parent structure. A reconstructive transformation is one in which the change in structure is achieved by a flow of matter, which occurs in such a way that strains are minimized.

All the transformations cause changes in shape (Fig. 5a), which for reconstructive transformations simply reflects the change in density. For displacive transformations, the shape change is an *invariant-plane strain* (IPS), that is, a combination of a shear on the invariant plane and a dilatation normal to that plane. The strain energy associated with a constrained IPS is minimized when the product phase has a thin-plate shape. This is why Widmanstätten ferrite, bainite, acicular ferrite, and martensite in steels grow in the form of plates. The distinguishing features of a variety of deformation modes are compared in Table 2, and Table 3 describes the shape deformations.

The permanent strain caused by any transformation is called *transformation plasticity*. A

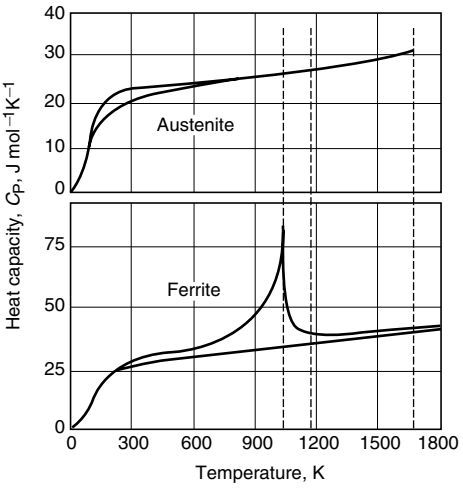

Fig. 2 Specific heat capacities of ferrite and austenite in pure iron, as a function of temperature. The thin lines represent the combined contributions of the phonons and electrons, whereas the thicker lines also include the magnetic terms. The dashed vertical lines represent the Curie, $\alpha \rightarrow \gamma$, and $\gamma \rightarrow \delta$ transitions. δ-ferrite is simply an alternative historical name for high temperature α. Source: Ref 5

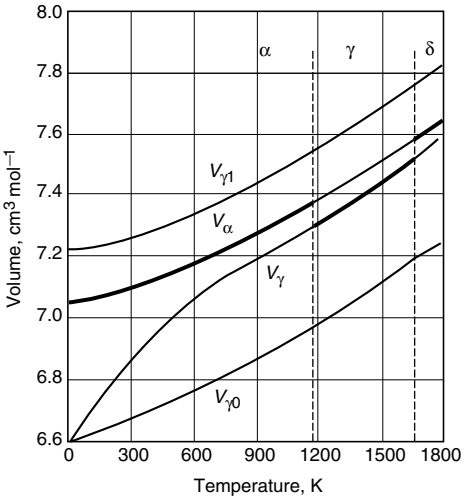

Fig. 3 Molar volumes of the various forms of iron. Source: Ref 5

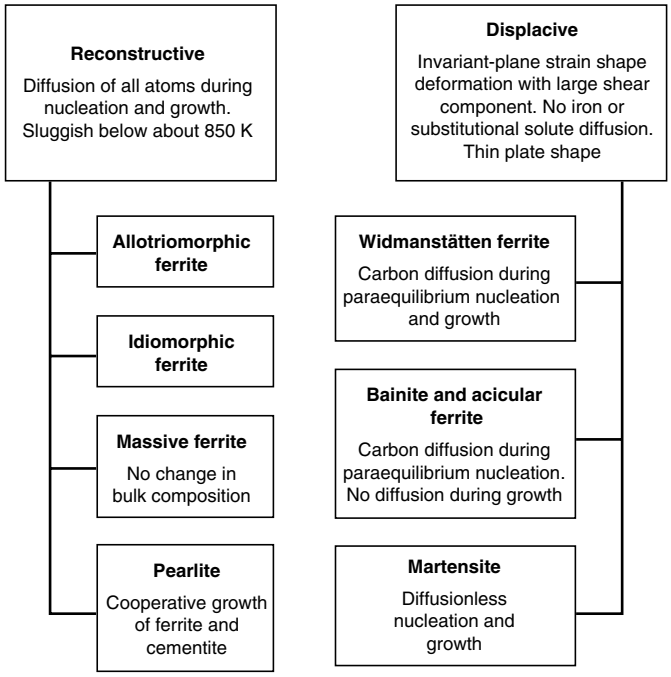

Fig. 4 Transformation products of austenite. Source: Ref 12

phase change in a stress-free material is usually triggered by heat treatment, when the parent phase passes through an equilibrium transformation temperature. Alternatively, the application of a stress in isothermal conditions can trigger transformation in circumstances where it would not otherwise occur. Unusual effects can occur when stress and temperature work together. The transformation may occur at remarkably low stresses or at very small deviations from the equilibrium temperature. This is why even minute stresses can greatly influence the development of microstructure, and vice versa. It is not surprising that transformation plasticity can be obtained at stresses that are much smaller than the conventional yield stress of the parent phase.

Transformations, Residual Stresses, and Related Phenomena

The strains due to phase transformations can alter the state of residual stress or strain. It is well known that the martensitic transformation of the carburized surface of a steel component puts the surface under compression. It is argued that this is because of the expansion at the surface due to formation of the lower-density martensite from austenite.

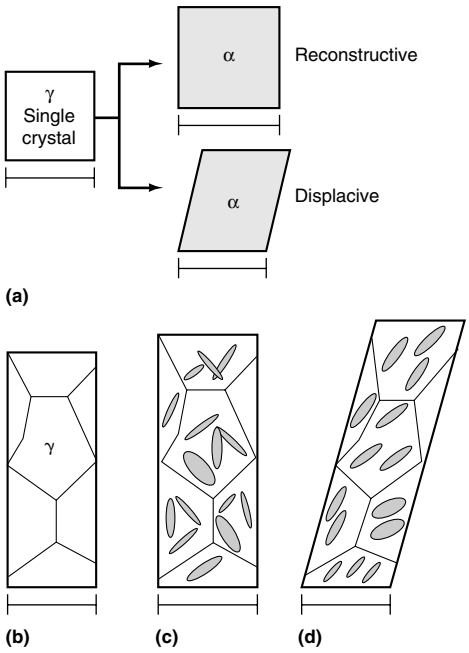

Fig. 5 Shape changes accompanying unconstrained transformations. Note that the horizontal scale bars are all the same length. (a) The two kinds of shape changes that occur when a single crystal of austenite transforms to a single crystal of ferrite, as a function of the mechanism of transformation. (b) Polycrystalline sample of austenite. (c) Polycrystalline sample of austenite that has partially transformed by a displacive transformation mechanism into a random set of ferrite plates. (d) Polycrystalline sample of austenite that has partially transformed by a displacive transformation mechanism into an organized set of ferrite plates.

Phase transformation can also compensate for stress. Greenwood and Johnson (Ref 13, 14) showed that when a phase change is accompanied by a change in volume, the tensile strain expected when transformation occurs under the influence of a tensile stress σ is given by:

$$\varepsilon = \frac{5}{6}\frac{\Delta V}{V}\frac{\sigma}{\sigma_Y} \qquad \text{(Eq 2)}$$

where σ_Y is the yield stress of the weaker phase and $\Delta V/V$ is the transformation volume strain. The role of shear strains associated with transformation has been emphasized in later work by Magee and Paxton (Ref 15, 16), and subsequently by Fischer (Ref 17), Leblond et al. (Ref 18–22), Olson (Ref 23), and Bhadeshia et al. (Ref 24). Not only does transformation affect stress, but the latter modifies the development of microstructure. The microstructure tends to be more organized when transformation occurs in a stress's parent phase, because the stress favors the formation of certain orientations relative to others. This is illustrated schematically in Fig. 5(b) to (d). These aspects will now be discussed in more detail, because transformation plasticity can radically alter the state of residual stress.

Deformation System

Displacive transformations can be regarded as modes of plastic deformation. Just as a combination of a plane and a direction constitutes a deformation system for slip or twinning, the habit plane and displacement vector of the invariant-plane strain accompanying displacive transformation completely describe the deformation system responsible for transformation plasticity. The displacement vector describes the sense of the macroscopic displacements accompanying transformation and, along with the habit plane indices, also contains information about the magnitude of the shear component and dilatational component of the displacements. Typical data for the deformation systems associated with transformations are listed in Table 4. Note that reconstructive transformations involve only a volume change together with diffusional mass flow, so it is not appropriate to regard them as deformation systems in the present context.

Given the cubic crystal structure, and the fact that habit planes tend to be irrational, there will in general be 24 of these systems per austenite grain, and they may operate simultaneously to varying extents. Of course, unlike ordinary slip,

Table 2 Characteristics of different modes of deformation

Characteristic	Slip deformation	Mechanical twinning	Displacive transformation	Reconstructive transformation
Causes permanent change in shape	Yes	Yes	Yes	Yes
Invariant-plane strain shape changewith a large shear component	Yes	Yes	Yes	No
Changes crystallographic orientation	No	Yes	Yes	Yes
Changes lattice type	No	No	Yes	Yes
Can lead to a density change	No	No	Yes	Yes

Table 3 Shape change due to transformation

Transformation	Shape change (a)	*s*(b)	δ(b)	Morphology
Allotriomorphic ferrite	Volume change	0.00	0.02	Irregular
Idiomorphic ferrite	Volume change	0.00	0.02	Equiaxed, faceted
Pearlite	Volume change	0.00	0.03	Spherical colonies
Widmanstätten ferrite	Invariant-plane strain	0.36	0.03	Thin plates
Bainite	Invariant-plane strain	0.22	0.03	Thin plates
Acicular ferrite	Invariant-plane strain	0.22	0.03	Thin plates
Martensite	Invariant-plane strain	0.24	0.03	Thin plates
Cementite plates	Invariant-plane strain?	0.21?	0.16?	Thin plates
Mechanical twins (α)	Invariant-plane strain	$1/\sqrt{2}$	0.00	Thin plates
Annealing twins (γ)		0.00	0.00	Faceted

(a) An invariant-plane strain here implies a large shear component as well as a dilatational strain normal to the habit plane. (b) *s* and δ refer to the shear and dilatational strains, respectively. The values stated are approximate and will vary slightly as a function of lattice parameters and the details of crystallography.

Table 4 Deformation systems associated with transformations

Phase	Habit plane indices	Displacement vector	*m*
Martensite	(0.363 0.854 0.373)	[$\overline{0.195}$ 0.607 $\overline{0.771}$]	0.185
Bainite	(0.325 0.778 0.537)	[0.159 0.510 $\overline{0.845}$]	0.27
Widmanstätten ferrite	(0.506 0.452 0.735)	[$\overline{0.867}$ 0.414 0.277]	0.36

Note: Typical habit plane and displacement directions for low-alloy steels. The indices all refer to the austenite phase. Note that the indices stated are approximate, since the habit plane and displacement direction are usually irrational. The displacement vector does not quite lie in the habit plane because the dilatational strain is directed normal to the habit plane. The magnitude of the displacement is given by m, which is the total displacement including the shear and the dilatational components.

the different deformation systems within an austenite grain cannot intersect, except in special circumstances where intervariant transformations are possible, as is the case with some shape-memory alloys. It follows that the ordinary notion of work hardening does not apply. Work hardening nevertheless manifests itself via a different mechanism, in which the stability of the austenite increases as it becomes ever more finely divided.

The Taylor/von Mises criterion (Ref 25, 26) states that in any given crystal, a minimum of five independent slip systems is necessary to produce an arbitrary shape change. A crystal in a polycrystalline aggregate has to accommodate the arbitrary deformations of neighboring grains. Therefore, a polycrystalline material is brittle unless each grain contains at least five independent slip systems. Similar logic can be applied to the crystallographic variants of a phase generated by displacive transformation. The habit plane is predicted theoretically (Ref 27, 28) and found experimentally (Ref 29) to have irrational indices. This means that there exist, in principle, 24 possible variants of the habit plane per grain of austenite (that is, 24 independent deformation systems). Given this large number of transformation variants available per grain, the Taylor criterion leads to the conclusion that transformation plasticity can cause, or accommodate, any externally imposed, arbitrary shape change—assuming that a sufficient quantity of parent phase is available. It follows that polycrystalline samples can remain intact at grain boundaries when transformation plasticity is the sole mode of deformation.

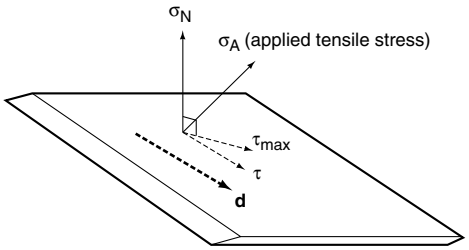

Fig. 6 Resolution of the applied stress, σ_A. The normal stress, σ_N, and the shear stress, τ, both act on the habit plane. The vector **d** is the direction along which lie the shear displacements of the shape deformation. τ_{max} is the maximum shear stress on the habit plane, but τ is given by resolving τ_{max} along **d**. Note that **d** differs slightly from the displacement vector of the IPS, which includes a dilatational component in addition to the shear.

Table 5 Typical values of the mechanical driving force coefficients

Nature of stress	$\partial\Delta G/\partial\sigma$, J/(mol MPa)
Uniaxial tension	−0.86
Uniaxial compression	−0.58
Elastic crack tip (a)	−1.42

(a) The stress state for the crack tip is multiaxial, but the coefficient is calculated by expressing the stress in terms of the von Mises equivalent tensile stress. Source: Ref 32

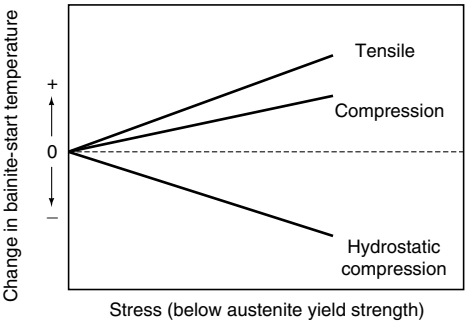

Fig. 7 Indication of how the transformation-start temperature (for Widmanstätten ferrite, bainite, acicular ferrite, or martensite) should vary as a function of the nature and magnitude of an applied stress whose magnitude is less than that of the yield stress.

Table 6 Sensitivity of transformation-start temperatures in steels to applied stress

Phase	Nature of stress	Sensitivity, K/MPa
Martensite	Pressure	−0.06
Bainite	Pressure	−0.09
Eutectoid	Pressure	−0.011
Martensite	Tensile	+0.06

Source: Ref 32

Mechanical Driving Force

The interaction of an applied elastic stress with a phase change can occur in two ways:

1. The stress can alter the driving force for the transformation.
2. The stress can change the appearance of the microstructure by favoring the formation of those variants which best comply with the applied stress.

For reconstructive transformations, only the hydrostatic component of stress can interact with the volume change. The corresponding interaction with displacive transformations is much larger because of the shear component of the IPS.

For displacive transformations, the influence of stress on the transformation can be expressed as a mechanical driving force (ΔG_{mech}), which is the work done by the external stress in producing the macroscopic shape deformation (Ref 30, 31):

$$\Delta G_{mech} = \sigma_N\delta + \tau s \quad \text{(Eq 3)}$$

where σ_N is the normal stress on the habit plane and τ is the component of the shear stress on the habit plane that is parallel to the direction along which the shear displacements of the shape deformation occur (Fig. 6). The strains δ and s are the dilatational and shear components, respectively, of the shape deformation. Some typical values of the mechanical driving force terms are given in Table 5. Given a free choice of some 12 to 24 crystallographic variants of the transformation product in each grain of austenite, the work done by the shear stress is always expected to be positive, whereas that due to the dilatational component depends on the sign of σ_N. For steels, this latter component is relatively small. Any observed consequences of stress must therefore reflect the dominant role of the shear component unless the stress is purely hydrostatic.

Since the shear stress remains positive irrespective of whether the sample is pulled in tension or uniaxially compressed, and since the shear component of the shape change is large, a uniaxial stress will always cause a temperature increase for displacive transformations in steels. Hydrostatic stress, on the other hand, has no deviatoric components and consequently interacts only with the dilatational component of the shape change. Thus, hydrostatic compression is expected and found to lead to a decrease in the transformation temperature (Fig. 7); some data (Ref 32) on the sensitivity of the transformation temperature to applied stress are presented in Table 6.

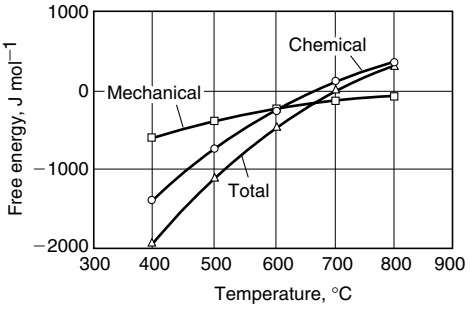

Fig. 8 Typical magnitudes of the chemical and mechanical driving forces for stress-affected transformation. The mechanical driving force is estimated for an applied stress that is equal to the yield stress of austenite. Since this yield stress becomes small at high temperatures, the contribution of the mechanical driving force also decreases. Therefore, transformation becomes impossible as the temperature exceeds about 700 °C (1290 °F).

Limits to Stress-Assisted Transformation

At temperatures close to that at which the equilibrium transformation occurs, an applied stress can assist reaction when the chemical driving force is insufficient to achieve the change on its own. There must exist a point, however, when the applied stress simply cannot provide enough mechanical driving force to complement the chemical term to give a driving force large enough to induce transformation. After all, the magnitude of the stress that can be applied is limited by the yield point of the parent phase. Thus, there are limits to what can be achieved by the application of stress as a stimulus to transformation (Fig. 8).

Transformation under Constraint: Residual Stress

Residual stresses are often introduced unintentionally during fabrication—for example, during welding or heat treatment. A few elegant experiments illustrate how phase transformations interact with the buildup of residual stress.

Using bainitic, martensitic, and stable austenitic steels, Jones and Alberry (Ref 33, 34) demostrated that transformation plasticity during the cooling of a uniaxially constrained sample from the austenite phase field acts to relieve the buildup of thermal stress as the sample cools. By contrast, the nontransforming austenitic steel exhibited a continuous increase in residual stress with decreasing temperature, as might be expected from the thermal contraction of a constrained sample.

When the steels were transformed to bainite or martensite, the transformation strain compensated for any thermal contraction strains that arose during cooling. Significant residual stresses were therefore found to build up only after transformation was completed and the specimens approached ambient temperature (Fig. 9).

The experiments contain other revealing features. The thermal expansion coefficient of austenite (1.8×10^{-6}/K) is much larger than that of ferrite (1.18×10^{-6}/K), and yet the slope of the line prior to transformation is smaller when compared with that after transformation is complete (Fig. 9). This is because the austenite yields to accommodate the thermal contraction, which is possible because the yield strength of the austenite is reduced at elevated temperatures. Ferrite is strong at low temperatures, so the slope of the stress/temperature curve (after transformation is complete) is steeper and consistent with the magnitude of thermal contraction strains.

Interpretation of experimental data of the kind illustrated in Fig. 9 is difficult in the region of the stress/temperature curve where transformation occurs. The popular view that the volume change due to transformation is the major component of transformation plasticity is probably incorrect for displacive transformations such as bainite or martensite. The shape change due to transformation has a shear component that is much larger than the dilatational term (Table 3). Admittedly, this shear component should, on average, cancel out in a fine-grained polycrystalline sample containing plates in many orientations (Fig. 5c). However, the very nature of the stress effect is to favor the formation of selected variants, in which case the shear component rapidly begins to dominate the transformation plasticity (Fig. 5d).

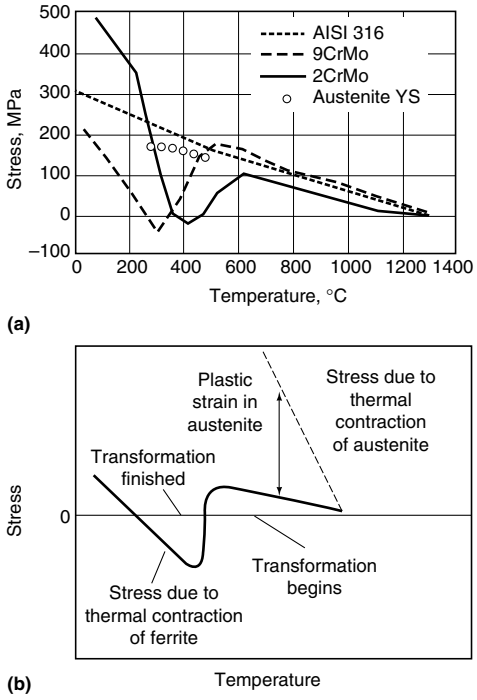

Fig. 9 (a) Plot of residual stress versus temperature for a martensitic (9CrMo), bainitic (2CrMo), and austenitic steel (AISI 316). Adapted from Ref 33, 34. (b) Interpretation of the Jones and Alberry experiments. The thermal expansion coefficient of austenite is much larger than that of ferrite.

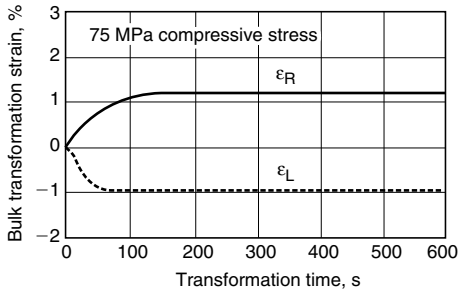

Fig. 11 Development of anisotropic transformation strain when bainite forms under the influence of a constant, elastic applied compressive stress. Note that the shear strain associated with the formation of one plate is about 26%, with a volume change of about 3%. The potential for anisotropy is therefore much greater than illustrated here.

The residual stress at ambient temperature is larger when the austenite finishes transformation at a high temperature. This is because thermal contraction strains can no longer be compensated by transformation plasticity once the austenite has decomposed. Low transformation temperatures help minimize residual stresses. High-strength welding alloys used for making submarine hulls therefore have transformation temperatures of less than about 250 °C (480 °F).

Figure 10 illustrates one kind of distortion found in welds, measured in terms of the angle θ through which the unconstrained plates rotate as they cool. Table 7 shows how the distortion depends on the temperature at which the majority of the transformation is completed, for two manual metal arc welds deposited with a 60° V-joint preparation in a multipass fabrication involving about 11 layers, with two beads per layer to complete the joint. The distortion is clearly larger for the case where the transformation is exhausted at the higher temperature.

Anisotropic Strain and Transformation Plasticity

When an unstressed polycrystalline sample of austenite is transformed to plates of ferrite, the shear caused as each randomly oriented plate forms is canceled on a macroscopic scale; only the volume expansion is observed experimentally. However, if the plates do not form at random—for example, when certain variants are favored because they comply better with the external stress—the shear strains are no longer canceled out. Transformation will then lead to highly anisotropic strains, as illustrated in Fig. 11. Naturally, any anisotropy will be greatest for displacive rather than reconstructive transformations, given that the former involve large shear strains.

Modeling Anisotropic Transformation Strains

Consider a distribution of bainite variants along all radial directions in a circle with the compression axis as its diameter (Ref 35, 36). The circle is divided into 18 equal segments (i $= 1 \rightarrow 18$), each segment representing a particular orientation of bainite habit plane. The choice of 18 segments is convenient and arbitrary. The compression axis of the sample is taken to be the z direction, the x and y directions

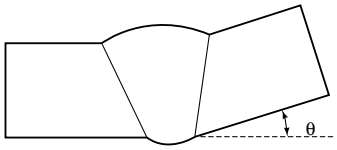

Fig. 10 Distortion caused by welding two plates that were originally flat

Table 7 Chemical composition, calculated transformation temperature range (ΔT), and measured distortion (θ) for two manual metal arc, multipass weld deposits

Composition, wt%							
C	Si	Mn	Ni	Mo	Cr	ΔT, °C(°F)	θ
0.06	0.5	0.9	. . .	. . .	. . .	802–400 (1476–750)	14.5
0.06	0.3	1.6	1.7	0.4	0.35	422–350 (792–660)	8

Source: H.K.D.H. Bhadeshia and L.-E. Svensson, unpublished data, 1994

being radially orientated; the unit vectors **x**, **y**, and **z** define the orthonormal basis X of the sample, giving a corresponding reciprocal basis X^*. The shear and dilatational components of the IPS accompanying the growth of bainite are approximately $s = 0.22$ and $\delta = 0.03$. Thus, the 3×3 deformation matrix describing the shape deformation is given by:

$$P = \begin{pmatrix} 1 + fse_1p_1 + f\delta p_1p_1 & fse_1p_2 + f\delta p_1p_2 & fse_1p_3 + f\delta p_1p_3 \\ fse_2p_1 + f\delta p_2p_1 & 1 + fse_2p_2 + f\delta p_2p_2 & fse_2p_3 + f\delta p_2p_3 \\ fse_3p_1 + f\delta p_3p_1 & fse_3p_2 + f\delta p_3p_2 & 1 + fse_3p_3 + f\delta p_3p_3 \end{pmatrix}$$

where p is the unit normal to the habit plane and e is the unit direction along which the shear occurs. This can be written more succinctly as:

$$P = I + fs\begin{bmatrix} e_1 \\ e_2 \\ e_3 \end{bmatrix}(p_1p_2p_3) + f\delta\begin{bmatrix} p_1 \\ p_2 \\ p_3 \end{bmatrix}(p_1p_2p_3)$$

where I is a 3×3 identity matrix. A further reduction of notation is achieved using the MacKenzie and Bowles notation (Ref 27):

$$(XP_iX) = I + f_is[X;e_i](p_i;X^*) + f_i\delta[X;p_i](p_i;X^*) \quad \text{(Eq 4)}$$

where the subscript i identifies a particular segment of interest and X and X^*, respectively, represent the real and reciprocal bases of the coordinate system in which the deformation is described. The notation due to MacKenzie and Bowles (Ref 27) is discussed in detail in Ref 35.

The components of the shear direction and the dilatation direction are given by:

$$[X;e_i] = f_i[-\cos(\theta_i)\ 0\ \sin(\theta_i)]$$

$$[X;p_i] = f_i[\sin(\theta_i)\ 0\ \cos(\theta_i)]$$

where θ_i represents the orientation of the habit plane of variant i and f_i is the volume fraction of bainite located in segment i.

A unit vector along the z direction changes to a new vector z' given by:

$$[X;z'] = \prod_{i=1}^{18} (XP_iX)\ [0\ 0\ 1]$$

whereas a unit vector along x changes to

$$[X;x'] = \prod_{i=1}^{18} (XP_iX)\ [1\ 0\ 0]$$

where $(x' - 1)$ and $(z' - 1)$ give the strains along the x and z directions. These are assumed to be equal to radial and longitudinal strains ε_R and ε_L, respectively.

It is expected that those segments that comply best with the applied stress transform most rapidly, whereas the others do so at a lower rate, or not at all. This can to some extent be incorporated into the model by calculating the energy change U_i as the stress interacts with the shape deformation of a particular variant (i). Patel and Cohen's method (Ref 30) gives:

$$U_i = \frac{\sigma}{2}[s \sin 2\theta_l \cos \phi_i + \delta(1 + \cos 2\theta_i)]$$

where ϕ is the angle between the shear direction and the direction of the shear component of the applied stress as resolved onto the habit plane. To facilitate a two-dimensional analysis, the value of ϕ_i is taken to be zero. A positive value of U_i adds to the chemical driving force ($\Delta G^{\alpha\gamma} = G^\gamma - G^\alpha$) for transformation; a negative value thus opposes transformation. Using these values of interaction energies, the model can be modified so that the segments transform in an order of decreasing U_i. There is, however, a further complication. The effect of stress should be largest when the interaction energy is large compared with the chemical driving force. To allow for this, the volume fraction f_i of each segment can be scaled according to the value of $U_i + \Delta G^{\alpha\gamma}$.

Note that for the model calculations, the transformation occurs with the most favored variants growing first (Fig. 12). The model thus exaggerates the effect of stress, since in reality, for the sort of stress levels considered experimentally, no variant is likely to be entirely suppressed. In addition, the grains in a polycrystalline sample are "randomly" oriented, so that perfect compliance with the applied stress is impossible. Nevertheless, the trends revealed by the model are expected to be correct.

The experimental data that need explaining, and their interpretation in terms of the model are summarized in Fig. 13 and may be stated as follows:

- Without any stress, in a random polycrystalline sample, the transformation strains are isotropic. This is easily understood since the shear components of randomly oriented plates tend to cancel out (Fig. 13a).
- The application of the small stress at a high transformation temperature (that is, a small chemical driving force) causes the development of anisotropic strains, the transverse strain first being negative and then positive (Fig. 13b). The same effect is observed for a large stress and low temperature (that is, a large driving force). The model explains this effect when it is assumed that the favored variants form first, but that the stress is not large enough to suppress the eventual formation of other variants. The signs of ε_L and ε_R are always opposite for the favored variants, but are identical for the rest of the variants. Therefore, the transverse strain is initially negative but then becomes positive as transformation progresses. The low-stress/high-temperature situation is equivalent to the high-stress/low-temperature case because in both of these circumstances, variants that are not favored cannot be suppressed. In the former case the stress is too small for suppression, whereas in the latter case the chemical driving force is too large to permit suppression.
- When a large stress is applied at a high temperature, the favored variants dominate. Therefore, the strains are always of opposite sign (Fig. 13c).

The model is thus capable of qualitatively explaining all the essential features of the formation of bainite under the influence of a small tensile stress. A uniaxial compressive stress (as used in the experiments described below) simply causes a reversal of the signs of the longitudinal and transverse stresses; there is also a minor effect from the unfavorable interaction between the compressive stress and the dilatational component of the IPS shape deformation.

The most interesting conclusion to emerge from comparison of the model with experimental data is that transformation under the influence of a mild stress occurs sequentially. Variants that comply with the applied stress grow first, fol-

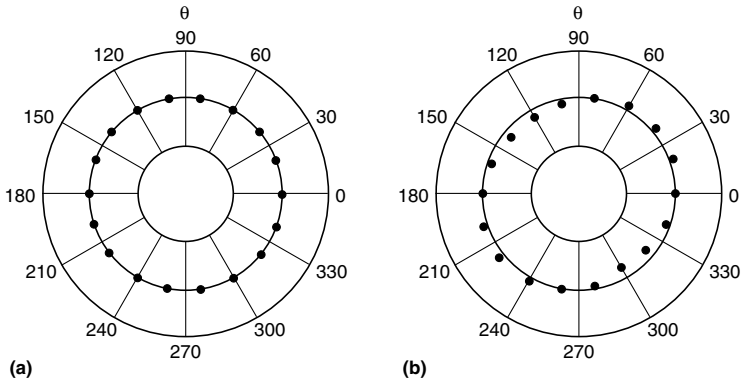

Fig. 12 Transformation behavior inherent in the model (Ref 36). The dots illustrate the area fraction of each segment, which in the calculations is scaled according to the value of $U_i + \Delta G^{\alpha\gamma}$. (a) Zero stress. All segments have equal area fraction, and the order in which they transform is irrelevant. (b) Applied stress of 40 MPa and $\Delta G^{\alpha\gamma} = 400$ J/mol. The area fractions of the segments are no longer equal. The segments in which the distance of the dot from the origin is largest transform first.

lowed by those that do not. This also carries the implication that the interaction of the stress is with the growth process (that is, the IPS shape deformation) rather than the strain field of the nucleus, which is likely to be different. It is worth noting that there are similar results for martensite: most favored variants grow first in the sequence of transformation under stress (Ref 15, 24).

Summary

Many of the thermal properties of steels—for example, heat capacity, thermal expansion coefficients, and latent heats of transformation—are remarkably well understood. Indeed, commercially available thermodynamic databases and programs can be used to estimate these quantities as a function of temperature and chemical composition. This capability has not been exploited in the analysis of residual stresses, even though phase diagram calculations using the same software are now routine in industry and academia.

Other properties, such as elastic modulus, are not yet calculable in the same manner. It may be the case that they are insensitive to alloying, but that remains to be demonstrated in the context of residual stress analysis.

There is little doubt that transformations in steel play a major role in the development of residual stresses. For reconstructive transformations (for example, pearlite), it is the difference in density between the parent and product phases that contributes to transformation plasticity. The plasticity can be much larger for displacive transformations (Widmanstätten ferrite, bainite, martensite) because of the large shear component of the shape deformation when these transformation products form. These are quite sophisticated effects which, with few exceptions, are not incorporated in most residual stress analyses.

REFERENCES

1. T. Inoue and Z. Wang, *Mater. Sci. Technol.,* Vol 1, 1985, p 845–850
2. P.W. Fuerschbach, in *The Metal Science of Joining,* M.J. Cieslak, J.H. Perepezko, S. Kang, and M.E. Glicksman, Ed., Minerals, Metals and Materials Society, 1992, p 21–30
3. R. Schröder, *Mater. Sci. Technol.,* Vol 1, 1985, p 754–764
4. L. Kaufman, E.V. Clougherty, and R.J. Weiss, *Acta Metall.,* Vol 11, 1963, p 323–335
5. L. Kaufman, in *Energetics in Metallurgical Phenomenon,* Vol III, W.M. Mueller, Ed., Gordon and Breach, 1967, p 55–84
6. K. Hack, Ed., *The SGTE Casebook: Thermodynamics at Work,* Institute of Materials, 1996
7. D.G. Pettifor and A.H. Cottrell, Ed., *Electron Theory in Alloy Design,* Institute of Materials, 1992
8. J.W. Christian, in *Decomposition of Austenite by Diffusional Processes,* V.F. Zackay and H.I. Aaronson, Ed., Interscience, 1962, p 371–386
9. H.M. Clark and C.M. Wayman, *Phase Transformations,* American Society for Metals, 1970, p 59–114
10. J.D. Watson and P.G. McDougall, *Acta Metall.,* Vol 21, 1973, p 961–973
11. J.W. Christian, "Physical Properties of Martensite and Bainite," Special Report 93, Iron and Steel Institute, 1965, p 1–19
12. H.K.D.H. Bhadeshia, *Bainite in Steels,* 2nd ed., Institute of Materials, 2001, p 1–453
13. G.W. Greenwood and R.H. Johnson, *Proc. Roy. Soc.,* Vol 238, 1965, p 403–422
14. R.H. Johnson and G.W. Greenwood, *Nature,* Vol 195, 1962, p 138–139
15. C.L. Magee, Ph.D. thesis, Carnegie Mellon University, 1966
16. C.L. Magee and H.W. Paxton, *Trans. Met. Soc. AIME,* Vol 242, 1968, p 1741–1749
17. F.D. Fischer, *Acta Metall. Mater.,* Vol 38, 1990, p 1535–1546
18. J.B. Leblond, G. Mottet, and J.C. Devaux, *J. Mech. Phys. Solids,* Vol 34, 1986, p 395–409, 411–432
19. J.B. Leblond, J. Devaux, and J.C. Devaux, *Int. J. Plasticity,* Vol 5, 1989, p 551–572
20. J.B. Leblond, *Int. J. Plasticity,* Vol 5, 1989, p 573–591
21. J.B. Leblond and J. Devaux, *Residual Stresses,* Elseviers, 1989, p 1–6
22. J.B. Leblond, *Internal Report CSS/L/NT/90/4022,* FRAMASOFT, 1990, p 1–12
23. G.B. Olson, *Deformation, Processing and Structure,* American Society for Metals, 1982, p 391–424
24. H.K.D.H. Bhadeshia, S.A. David, J.M. Vitek, and R.W. Reed, *Mater. Sci. Technol.,* Vol 7, 1991, p 686–698
25. R. Von Mises, *Z. Angew. Math. Mech.,* Vol 8, 1928, p 161
26. G.I. Taylor, *J. Inst. Met.,* Vol 62, 1928, p 307
27. J.K. MacKenzie and J.S. Bowles, *Acta Metall.,* Vol 2, 1954, p 138–147
28. M.S. Wechsler, D.S. Lieberman, and T.A. Read, *Trans. Amer. Inst. Min. Metall. Eng.,* Vol 197, 1953, p 1503–1515

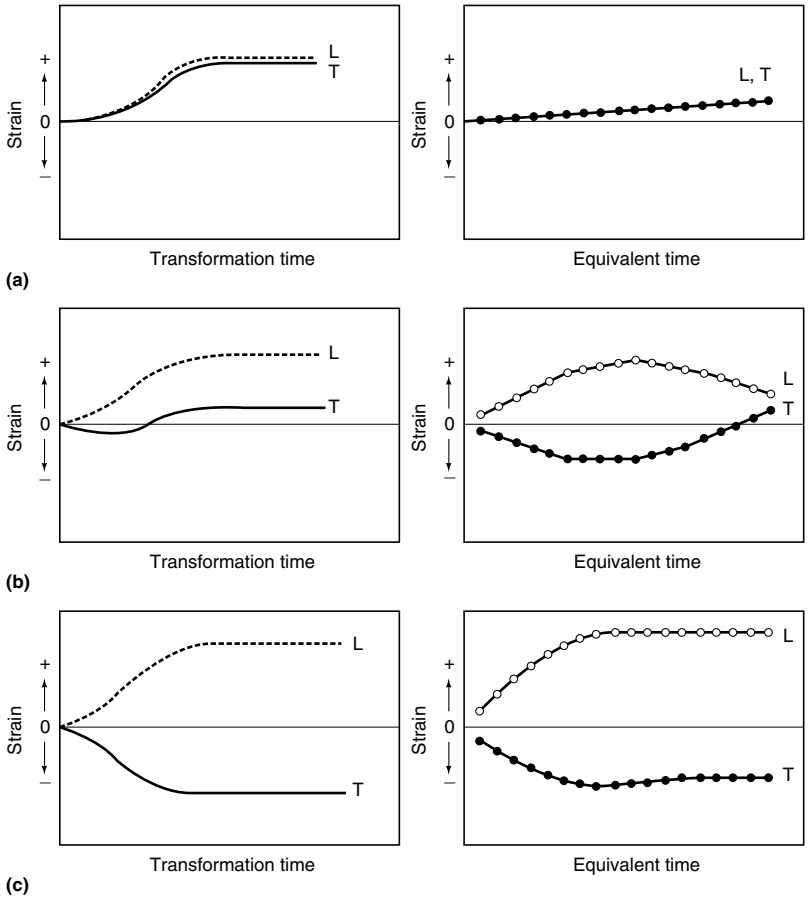

Fig. 13 Schematic of the reported variations (Ref 24) in longitudinal and radial strains during the isothermal formation of bainite under the influence of a tensile load, presented alongside predictions (Ref 36) from the crystallographic/thermodynamic model. The stresses are all intended to be below the austenite yield strength, and the data in this case refer to uniaxial tension. (a) Zero stress, any temperature. (b) Small stress, low temperature. (c) Small stress, high temperature; or large stress, low temperature.

29. A.B. Greninger and A.R. Troiano, *Trans. Amer. Inst. Min. Metall. Eng.,* Vol 140, 1940, p 307–336
30. J.R. Patel and M. Cohen, *Acta Metall.,* Vol 1, 1953, p 531–538
31. L. Delaey and H. Warlimont, in *Shape Memory Effects in Alloys,* J. Perkins, Ed., TMS-AIME, Plenum Press, 1975, p 89–114
32. S. Denis, E. Gautier, A. Simon, and G. Beck, *Mater. Sci. Technol.,* Vol 1, 1985, p 805–814
33. W.K.C. Jones and P.J. Alberry, *Ferritic Steels for Fast Reactor Steam Generators,* British Nuclear Engineering Society, 1977, p 1–4
34. W.K.C. Jones and P.J. Alberry, *Residual Stresses in Welded Constructions,* Welding Institute, 1977, Paper 2
35. H.K.D.H. Bhadeshia, *Worked Examples in the Geometry of Crystals,* Institute of Metals, 1987
36. A. Matsuzaki, H.K.D.H. Bhadeshia, and H. Harada, *Acta Metall. Mater.,* Vol 42, 1994, p 1081–1090

ASM International is the society for materials engineers and scientists, a worldwide network dedicated to advancing industry, technology, and applications of metals and materials.

ASM International, Materials Park, Ohio, USA
www.asminternational.org

Publication title	Product code
Handbook of Residual Stress and Deformation of Steel	06700G

To order products from ASM International:

Online Visit www.asminternational.org/bookstore

Telephone 1-800-336-5152 (US) or 1-440-338-5151 (Outside US)

Fax 1-440-338-4634

Mail Customer Service, ASM International
9639 Kinsman Rd, Materials Park, Ohio 44073, USA

Email Cust-Srv@asminternational.org

In Europe American Technical Publishers Ltd.
27-29 Knowl Piece, Wilbury Way, Hitchin Hertfordshire SG4 0SX, United Kingdom
Telephone: 01462 437933 (account holders), 01462 431525 (credit card)
www.ameritech.co.uk

In Japan Neutrino Inc.
Takahashi Bldg., 44-3 Fuda 1-chome, Chofu-Shi, Tokyo 182 Japan
Telephone: 81 (0) 424 84 5550